New methods for the calculation of the load capacity of bevel and hypoid gears

Prof. Dr.-Ing. Bernd-Robert Höhn[a], Prof. Dr.-Ing. Karsten Stahl[b], Dr.-Ing. Christian Wirth[c]

FZG-Forschungsstelle für Zahnräder und Getriebebau, Technical University of Munich, Boltzmannstraße 15, 85748 Garching, Germany

[a] hoehn@fzg.mw.tum.de, [b] stahl@fzg.mw.tum.de, [c] wirth@fzg.mw.tum.de

Keywords: bevel gears, hypoid gears, load capacity, calculation method, tooth contact analysis

1 Introduction

Hypoid gears are bevel gears with nonintersecting axes where the hypoid offset is defined as the shortest distance between these two axes. Hypoid gears are preferred over bevel gears without offset if aspects of gear noise or of installation space are in focus. Pitting and tooth root breakage are still the two most frequent failure types occurring in practical applications of bevel and hypoid gears. There are several national and international standards for the calculation of the load capacity of these gears such as DIN 3991 [1], AGMA 2003 [2] and ISO 10300 [3]. But up to now these standards do not cover bevel gears with offset (hypoid gears). For this reason a research project was carried out at FZG (Gear Research Centre, Munich, Germany) to analyse the influence of the hypoid offset on the load capacity. A new calculation method should be developed that is in principle based on the current version of ISO 10300 [3] but also valid for hypoid gears.

Although the load capacity of bevel gears has been investigated in several research projects at the FZG (Paul [4], Vollhüter [5], Fresen [6]), the isolated influence of the hypoid offset on pitting and bending could not be evaluated reliably, because the type of failure was changing on the corresponding test gears from tooth root breakage to pitting with an increasing offset. Thus, neither bending nor pitting could be investigated isolated regarding the influence of the hypoid offset. So, the main target of this project was the systematic investigation of the influence of the hypoid offset on the pitting and bending load capacity by means of two different types of test gears that fail either with pitting or tooth root breakage over the whole regarded offset range. Additionally the former test results were also taken into account to evaluate the new calculation method.

2 Experimental tests

For the experimental investigations two types of bevel gears were designed, one for the pitting tests and one for the tooth root tests. The aim of the two different gear designs was to examine pitting isolated from tooth root breakage. Thus, the gears for the tooth root tests were designed with offsets a = 0 / 15 mm / 31.75 mm with a relatively small module (m_{mn} = 2,2…2,5 mm), the gears for the pitting tests with offsets a = 0 / 15 mm / 31,75 mm / 44 mm with a bigger module (m_{mn} = 3,5…4,2 mm). All wheels had the same outer diameter d_{e2} = 170 mm. The gear sets were made of 18CrNiMo7-6 case hardened and finish ground. For each geometry the S/N-curve was determined by approximately 20 tests.

2.1 Results of the pitting tests

On each examined variant pitting occurred isolated from tooth root breakage. Beside the pitting failures micro pitting appeared. With increasing offset, the micro pitting area on the flank grew faster and bigger. **Fig. 1** shows typical pittings on the pinion flanks for all four examined test gear

geometries. In **Fig. 2** (left side) a pinion flank of the geometry variant with a = 15 mm is shown after 11 and 27 million pinion revolutions at T_1 = 300 Nm.

It was proven that the flank form deviation which occurs due to micro pitting affects the load distribution on the flank during the lifetime. This leads to locally changing load conditions and thus influences pitting. In test with torques close to the endurance limit of the gear set micro pitting had a larger influence because of the large runtime.

At the geometry variant with a = 0 mm (non hypoid) micro pitting occurred mainly at the dedendum of the flank, whereas for the hypoid variants (a = 15 mm / a = 31.75 mm / a = 44 mm) micro pitting could be documented over the whole active flank. The same applies to pitting.

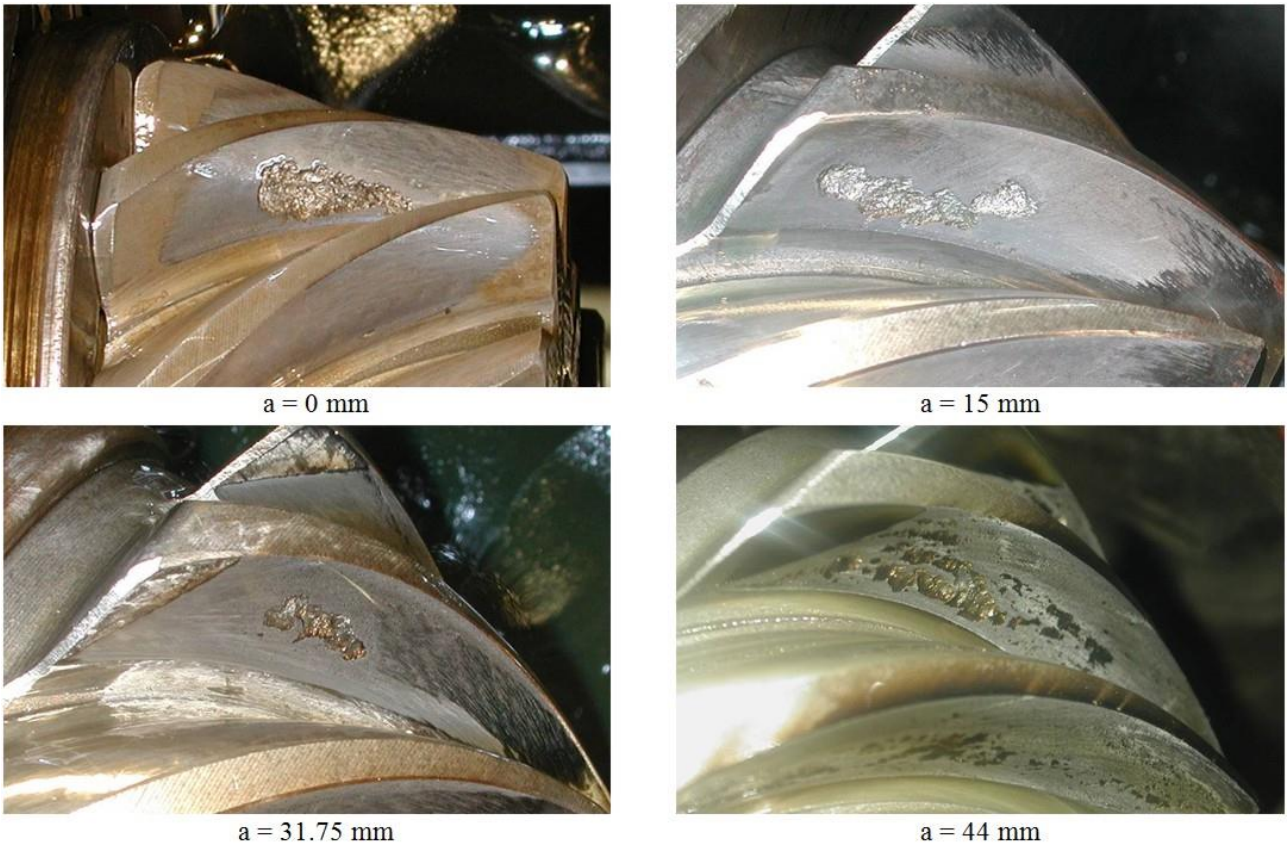

Fig. 1: Typical pitting at the pinion flanks on the investigated test gears

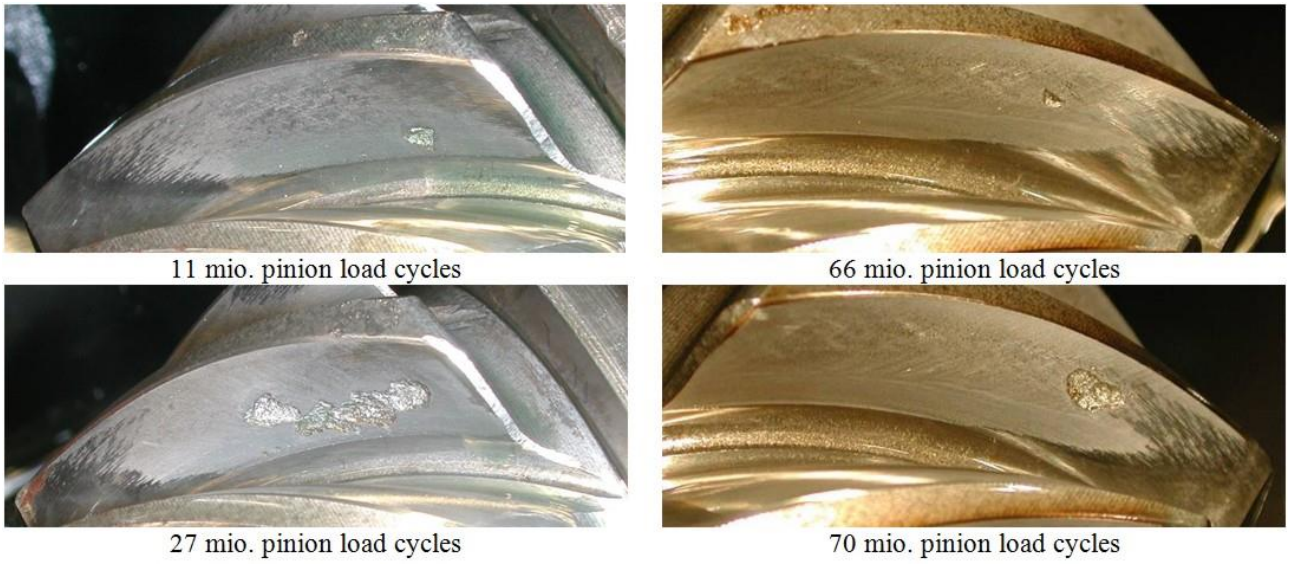

Fig. 2: left: micro pitting and pitting on pinion flank (T_1 = 300 Nm, a = 15 mm)
right: initial pitting at the addendum of the pinion toe (T_1 = 300 Nm, a = 15 mm)

On the right side of Fig. 2 the condition of the pinion flank (a = 15 mm) is shown for two different running times. Micro pitting could affect pitting in such way that the initial pitting occurs also at the addendum of the toe which is in contrast to helical gears. At commonly used helical gears micro pitting occur almost always below the pitch point at the dedendum of the pinion.

Although on the wheel flanks of the hypoid variant with an offset a = 44 mm pitting was also detected, it was not possible to evaluate the load capacity of the wheels because of the very few numbers of failures.

Fig. 3 shows the endurance limit for pitting for all tested variants. For each torque the maximum Hertzian stress was calculated by means of a loaded tooth contact analysis (LTCA) with BECAL [7]. BECAL [7] (Bevel Gear Calculation) was developed by the FVA (Forschungsvereinigung Antriebstechnik). It considers the deflections between pinion and wheel, which are caused by the elasticity of the teeth, bearings, shafts and housings. In contrast to the increasing pinion endurance torques the occurring maximum stresses on the flanks are decreasing. For example the maximum stress on the flank of variant a = 44 mm for the endurance limit is 22% smaller than that of the non-hypoid variant.

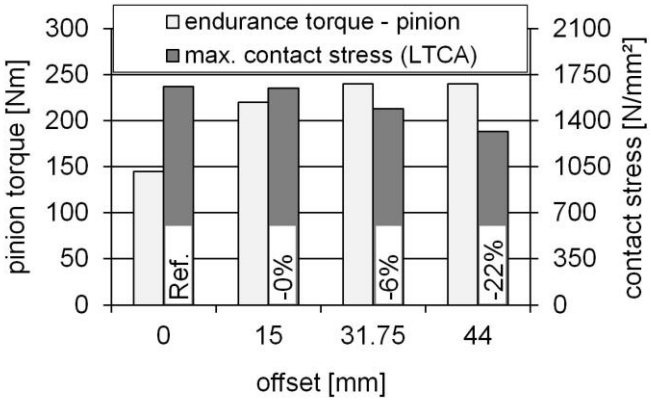

Fig. 3: Endurance limits of the test gears (pitting)

2.2 Results of the tooth root tests

All examined variants failed by the tooth root breakage. **Fig. 4** shows a tooth root breakage on a pinion that can be regarded as representative for all tests. The crack initiation was detected in all cases close to the 30°-tangent to the tooth fillet as it can be seen in **Fig. 5**.

Fig. 4: Typical tooth root breakage (a = 0 mm)

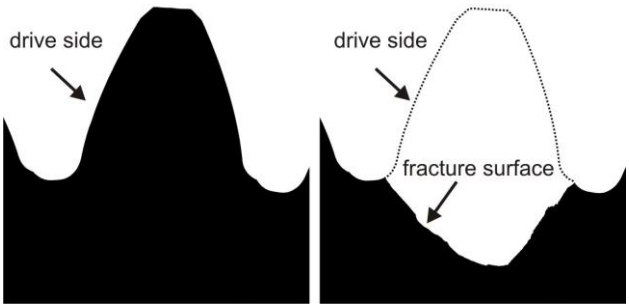

Fig. 5: Typical fracture surface (a = 0 mm)

In **Fig. 6** the endurance limits of the tested variants are compared. As expected the tests showed an increasing load capacity with higher offsets. The corresponding maximum tooth root stresses are for all variants within a range of ± 3.5%.

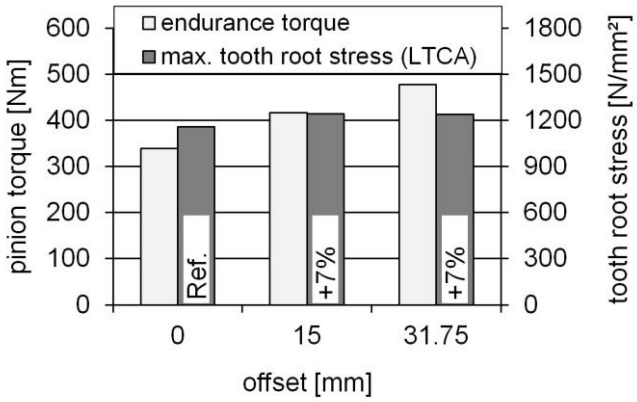

Fig. 6: Endurance limits of the test gears (bending)

3 New calculation method for bevel and hypoid gears

3. 1 Virtual cylindrical gear

In all widely used standard methods or standard capable methods the load capacity is determined by means of virtual cylindrical gears. Ideally the virtual gears have the same load capacity as the hypoid or bevel gear. Whereas for bevel gears without offset there is in principal only one solution for the virtual gears, hypoid gears can be transferred in diverse virtual gears. One reason for that are the two different spiral angles on hypoid gears whereby the pinion spiral angel and the gear spiral angle differ due to the offset angle. Eq. (1) to (6) are for the determination of the virtual cylindrical gear geometry. The derivation of the fundamental magnitudes will be explained in the following.

Reference diameter, d_v

$$d_{v1,2} = \frac{d_{m1,2}}{\cos\delta_{1,2}} \quad (1)$$

Tip diameter, d_{va}

$$d_{va1,2} = d_{v1,2} + 2\,h_{am1,2} \quad (2)$$

Root diameter, d_{vf}

$$d_{vf1,2} = d_{v1,2} - 2\,h_{fm1,2} \quad (3)$$

Helix angle, β_v

$$\beta_v = \frac{\beta_{m1} + \beta_{m2}}{2} \quad (4)$$

Base diameter, d_{vb}

$$d_{vb1,2} = d_{v1,2}\cos\alpha_{vet} \quad (5)$$

transverse effective pressure angle, a_{vet}

$$\alpha_{vet} = \arctan\left(\tan\alpha_e / \cos\beta_v\right)$$

$$\alpha_e = \alpha_{eD} \quad \text{for drive side (see ISO 23509)}$$
$$\alpha_e = \alpha_{eC} \quad \text{for coast side (see ISO 23509)} \quad (6)$$

Transverse base pitch, p_{vet}

$$p_{vet} = \pi\, m_{mn} \cos\alpha_{vet} / \cos\beta_v \quad (7)$$

Length of path of contact, $g_{v\alpha}$

$$g_{v\alpha} = \frac{1}{2}\left[\left(\sqrt{{d_{va1}}^2 - {d_{vb1}}^2} - d_{v1}\sin\alpha_{vet}\right) + \left(\sqrt{{d_{va2}}^2 - {d_{vb2}}^2} - d_{v2}\sin\alpha_{vet}\right)\right] \quad (8)$$

In **Fig. 7** the hypoid schematic with the pinion and wheel pitch cones is shown. Both pitch cones are tangent to the common pitch plane T. The surface lines of each pitch cone that are part of the pitch plane T enclose the offset angle ζ_{mp} in the calculation point P. The shortest distance between the axis of the pitch cones is defined as the hypoid offset a. If a = 0, then the pitch apexes are congruent and pinion and wheel have the same spiral angle.

For the proposed method it was the aim to generate the virtual cylindrical gears directly from the hypoid gear geometry without having any step in between (see **Fig. 8**). Furthermore the mesh

conditions of the virtual gears should represent those of the hypoid gears as close as possible. To find the solution of a suitable virtual gear comprehensive investigation inter alia by means of a loaded tooth contact analysis (LTCA) were made. The LTCA was done by the program BECAL [7]. With a special program the correlation between important geometry values as well as between essential magnitudes for the load capacity were analysed. Some will be explained in the following.

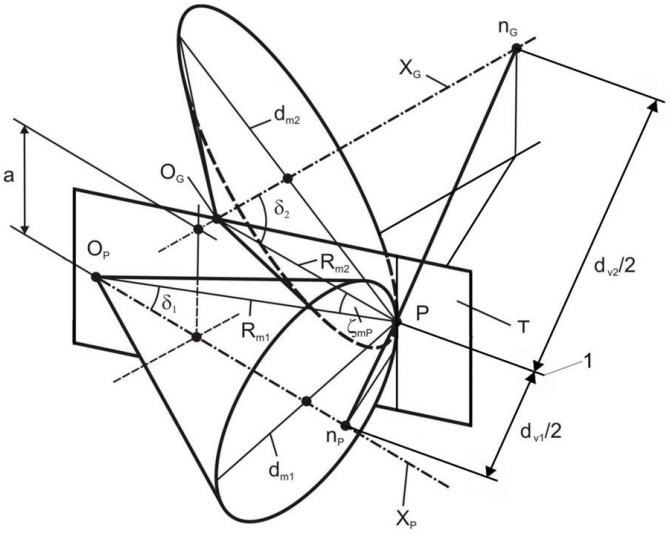

Fig. 7: Schematic of hypoid gear

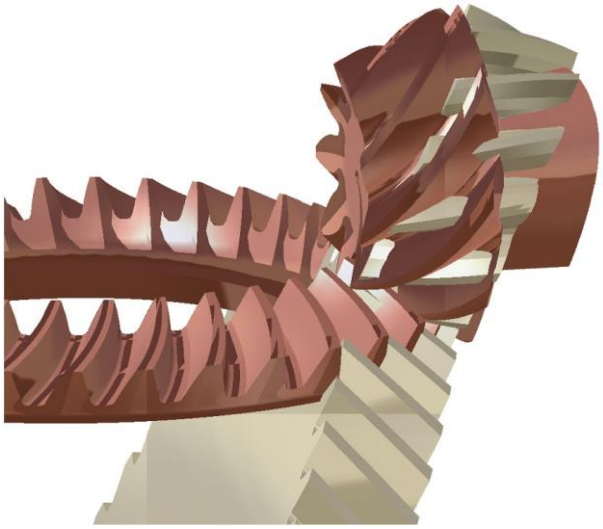

Fig. 8: Hypoid gear and its virtual cylindrical gear

As described by [8] and [9] hypoid gears may have unequal mesh conditions on drive side and coast side flank if the value of the limit pressure angle α_{lim} is different from zero (for bevel gears: $\alpha_{lim} = 0$) . As **Fig. 9** illustrates the normal forces F_{ntD} and F_{ntC} in profile section on both flank sides are inclined from the pitch plane by the (generated) pressure angles α_{tD} and α_{tC}. The projections of the zones of action are inclined by the effective pressure angle α_{etD} and α_{etC}. If $\alpha_{lim} \neq 0$ then the direction of the normal forces on the flank are inclined against the zone of action. If the generated pressure angles are equal ($\alpha_{tD} = \alpha_{tC}$, e.g. Zyklo-Palloid, Klingelnberg) then the lengths of the zone of action for drive and coast side are unequal. Furthermore the radius of relative curvature is different on both flank sides what effects the occuring Hertzian stresses. To balance the mesh conditions the generated pressure angles have to be chosen unequal regarding α_{lim} according to ISO 23509 [10]. It is obvious that the effect described has to be considered in the virtual cylindrical gear, if the mesh conditions of the hypoid gear should be mapped.

The derivation of the pitch diameters of the virtual cylindrical can be seen in Fig. 9 where a hypoid gear with an offset of a = 31.75 mm and an outer diameter of d_{e2} = 170 mm is regarded. The full lines are the projections of the tip-, root- and pitch cones of pinion and wheel in axial plane of the virtual gears. Although the offset is considerable high the tip-, root- and pitch cylinders of the virtual gear acc. to eq. (1) to (3) (dotted lines) approximate the corresponding projections of the cone in the area of contact quite well.

The length of path of contact regards as mentioned before the influence of the limit pressure angle. The example shown in **Fig. 10** demonstrates how the length of path of contact is increasing on the coast side and is decreasing on the drive side if the offset is increased and the generated pressure angles are kept constant to $\alpha_n = 20°$. For an offset a = 30 mm the limit pressure angle is $\alpha_{lim} = -9.87°$. The values for the black lines are determined by a LTCA, the grey lines represent the values for the virtual cylindrical gears according to eq. (8). Whereas Niemann/Winter III [11] does not regard the effects of the limit pressure angle the new virtual gear gives a good correlation to the LTCA.

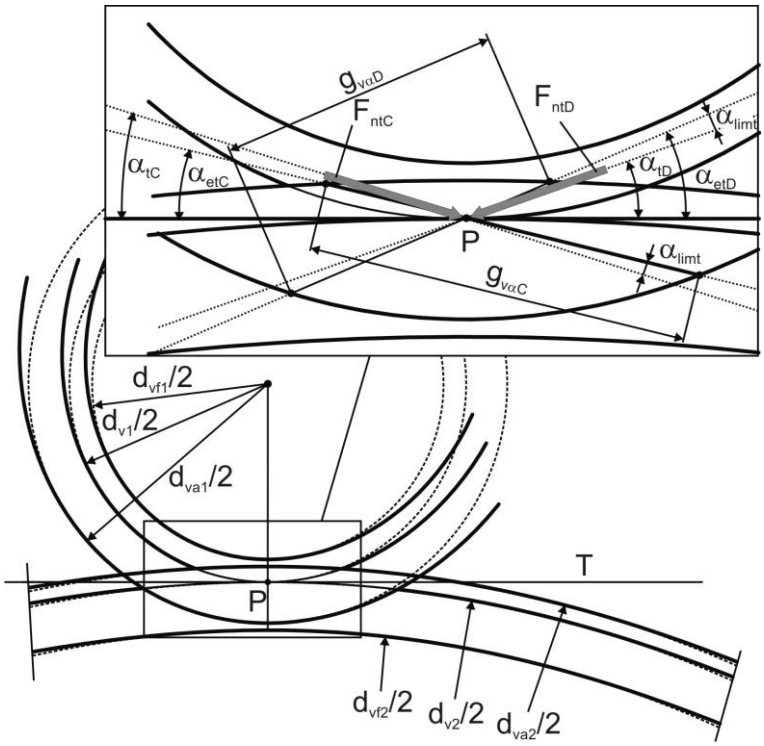

Fig. 9: Asymmetric mesh conditions on hypoid gears

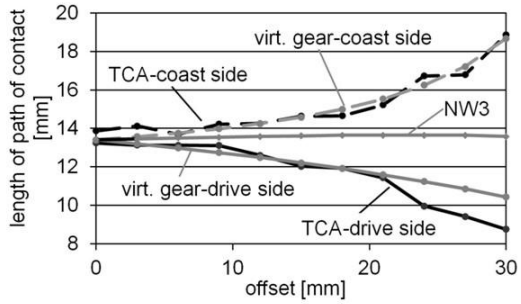

gear type		Zyklo-Palloid
gear ratio	z_1 / z_2	9 / 34
wheel mean spiral angle	β_{m2}	33°
wheel outer diameter	d_{e2}	170 mm
wheel face width	b_2	26 mm
pinion profile shift coeff.	x_{hm1}	0,65
gen. pressure angle	α_n	20°

Fig. 10: Length of path of contact over hypoid offset

To represent the mesh conditions of the hypoid gears it is not less important to approximate the shape of the contact zone as good as possible. However the complexity of the derivation has to be limited in order to keep the method capable for a standard. ISO 10300 [3] assumes to have an elliptical contact zone, DIN 3991 [1] implies a rectangular contact zone. For the new method the shape of the contact zone is approximated by a parallelogram. Based on comprehensive studies regarding the contact zones of conventional hypoid gears it seemed to be adequate compromise. The enclosed angles of the parallelogram are dependent to the hypoid offset. For bevel gears (a = 0) the parallelogram becomes a rectangle. The derivation of the parallelogram is based on semi-empirical coherences that are shown in **Fig. 11**.

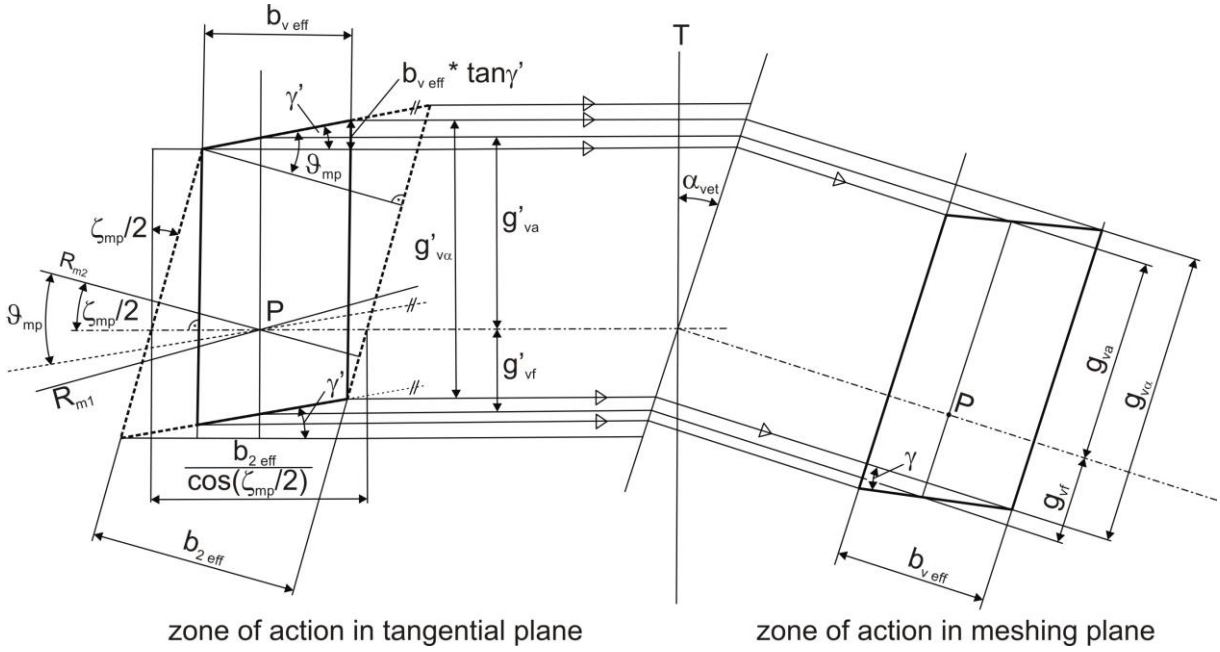

Fig. 11: Simplified zone of action for virtual cylindrical gears

Whereas the face width of virtual cylindrical gears and of their pertaining bevel gears without offset have the same size ($b_v = b$), this is not true for hypoid gears. Before the face width b_v can be calculated, the effective face width $b_{v\,eff}$ of the virtual cylindrical gear pair has to be determined. For that purpose, the length of the contact pattern $b_{2\,eff}$ which is measured in the direction of the wheel face width, is used. It is assumed that the theoretical zone of action of the hypoid wheel is not arched but developed into a parallelogram and then projected onto the common pitch plane T as shown in Fig. 11 by fat dotted lines. The side lines of this zone of action around mean point P are vertical to the wheel axis which in this view coincides with the cone distance R_{m2}. The other two boundary lines are parallel to the instantaneous axis of helical relative motion of the hypoid gear pair which is given by the angle ϑ_{mp}.

The zone of action of the corresponding virtual cylindrical gear pair is the greatest possible parallelogram (fat lines in Fig. 11) inscribed in the theoretical zone of action of the wheel whereby the side lines now are vertical to the axis of roll of the virtual cylindrical gear pair given by the angle $\zeta_{mp}/2$. The width of this smaller parallelogram appears in the given view in true length and it is the effective face width $b_{v\,eff}$ of the virtual cylindrical gear pair. To get the complete zone of action in true size the given top view is projected into the plane inclined by the effective pressure α_{vet} of the active flank in which the path of contact is also in true size (see Fig. 11 on the right).

Effective face width, $b_{v\,eff}$

$$b_{v\,eff} = \frac{\left(b_{2\,eff}/\cos\left(\zeta_{mp}/2\right) - g_{v\alpha}\cos\alpha_{vet}\tan\left(\zeta_{mp}/2\right)\right)}{1-\tan\gamma'\tan\left(\zeta_{mp}/2\right)} \qquad (9)$$

with:

$$\gamma' = \vartheta_{mp} - \zeta_{mp}/2 \qquad (10)$$

$$\vartheta_{mp} = \arctan\left(\sin\delta_2\tan\zeta_m\right) \qquad (11)$$

for δ_2, ζ_{mp} and ζ_m see ISO 23509 [10]

Face width, $b_{v\,eff}$

$$b_v = b_2\frac{b_{v\,eff}}{b_{2\,eff}} \qquad (12)$$

$b_{2\,eff}$ is the effective width of the contact pattern under a certain load. It has to be derived from measurements or tooth contact analysis, at the preliminary design stage by estimation.

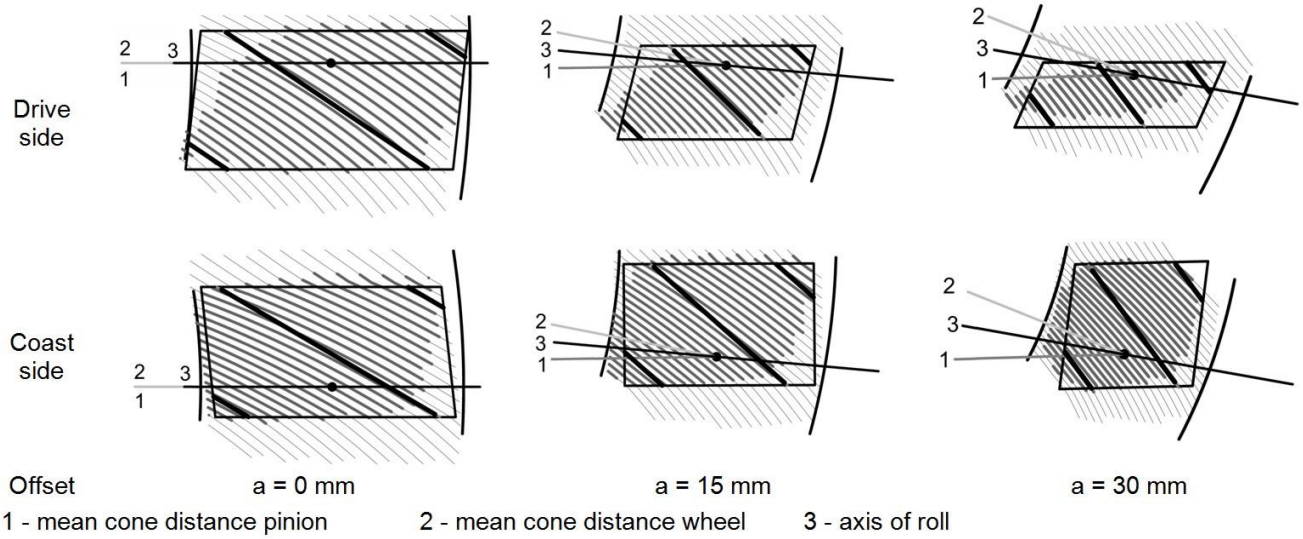

Fig. 12: Exemplary zones of action of virtual cylindrical gear pairs and calculated contact patterns of the bevel gear sets in a projection parallel to the wheel axis

The parallelogram as zone of action determined for the virtual cylindrical gear pair is now compared with the contact lines and pattern calculated by a LTCA. The regarded gear sets correspond to those calculated in Fig. 10. **Fig. 12** shows zones of action of 3 sets with different offset values (drive side and coast side) projected into a plane vertical to the wheel axis. As a reference, in each plot is given the axis of roll of virtual cylindrical gears and the lines of mean cone distances of pinion and wheel which intersect in the respective mean point P. Additionally, the parallelogram of the virtual zone of action contains three representative straight contact lines. They fit angularly very well with the calculated curved contact lines which are drawn thicker where they form the contact pattern. And each of these calculated contact patterns is well covered in size and position by the parallelogram of the respective virtual cylindrical gears, which means that the equivalence of the meshing conditions between bevel gears and their virtual cylindrical gears is sufficient for a rating system. Hence it is possible to determine some fundamental values like the length of contact lines, the load sharing, the overlap ratio, etc. by considering this approach.

For the calculation of load capacity the applied load on one tooth in the critical mesh position has to be known. In ISO 10300 [3] the load sharing factors Z_{LS} and Y_{LS} account for load sharing between two or more pairs of teeth. The principle for the determination of the load sharing ratio was kept but adapted to the shape of the zone of action.

The load distribution along each contact line in the zone of action is assumed to be elliptical. The area, *A*, of each semi-ellipse (see **Fig. 13**) represents the load on the respective contact line, and the sum of all areas over all contact lines being simultaneously in mesh, represents the total load on the gear set. Additionally, the distribution of the peak loads, *p*, over contact lines is assumed to be a parabola (exponent *e*). On this basis the maximum load over the middle contact line divided by the total load is a measure for load sharing.

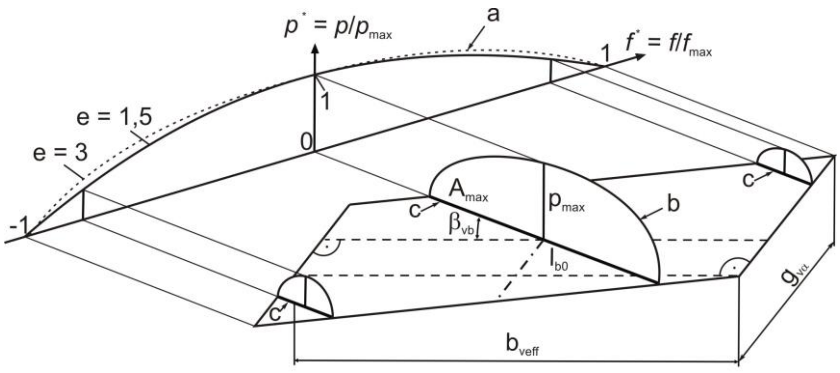

Fig. 13: Load distribution in the contact area

The radius of relative curvature in the decisive point of load application effects directly the occurring contact stress. Although there is no analytical solution for the radius of relative curvature in the contact of the flanks of a hypoid gear an acceptable approach has to be found for the rating system. Again the principle of ISO 10300 [3] was kept to get the relative curvature radius in the decisive point of load application. This means that like in ISO 10300 [3] in a first step the curvature radius for the mean point P is determined and then converted to the decisive point by the mid-zone factor $Z_{M\text{-}B}$ in a second step, whereby the value of $Z_{M\text{-}B}$ is calculated on the virtual cylindrical gear. Eq. (15) and (16) calculate the radius of relative curvature ρ_t in the mean point P in a normal section which is perpendicular to the pitch plane. The formula was derived by Shtipelman [8]. To get the decisive radius of relative curvature perpendicular to the contact line ρ_{rel} eq. (13) has to be considered. Of course the result for bevel gears without offset is equivalent to ISO 10300 [3] or DIN 3991 [1].

Radius of relative curvature vertical to the contact line, ρ_{rel}

$$\rho_{rel} = \rho_t \cos^2\beta_B \quad (13)$$

Inclination angle of contact line, β_B

$$\beta_B = \arctan(\tan\beta_v \sin\alpha_e) \quad (14)$$

Drive side:

$$\rho_t = \left[\frac{1}{\cos\alpha_{nD}(\tan\alpha_{nD} - \tan\alpha_{lim}) + \tan\zeta_{mp}\tan\beta_B} \frac{\cos\beta_{m1}\cos\beta_{m2}}{\cos\zeta_{mp}} \cdot \left(\frac{1}{R_{m2}\tan\delta_2} + \frac{1}{R_{m1}\tan\delta_1} \right) \right]^{-1} \quad (15)$$

Coast side:

$$\rho_t = \left[\frac{1}{\cos\alpha_{nC}(\tan(-\alpha_{nC}) - \tan\alpha_{lim}) - \tan\zeta_{mp}\tan\beta_B} \frac{\cos\beta_{m1}\cos\beta_{m2}}{\cos\zeta_{mp}} \cdot \left(\frac{1}{R_{m2}\tan\delta_2} + \frac{1}{R_{m1}\tan\delta_1} \right) \right]^{-1} \quad (16)$$

Fig. 14 shows a comparison of the radius of relative curvature for the drive and coast side flanks of the gears with the geometry acc. to Fig. 10. The black graphs represent the results from the TCA, whereas the grey lines show the radii of relative curvature that were calculated by the new rating method. The radii of relative curvature in the mean point ρ_P are compared by the dotted lines, the respective values in the decisive point of load application $\rho_{M\text{-}B}$ are represented by the filled lines. As it can be seen the differences are comparably small on both sides of the flank. Because of the flank form modifications (Ease-Off) that are not considered in the standard capable method, the values determined by TCA are somewhat smaller. It is remarkable that due to unequal mesh conditions on both flank sides the relative curvature radii are stronger increasing on the drive side. As the comparison shows this effect it is regarded sufficiently by the new standard capable method.

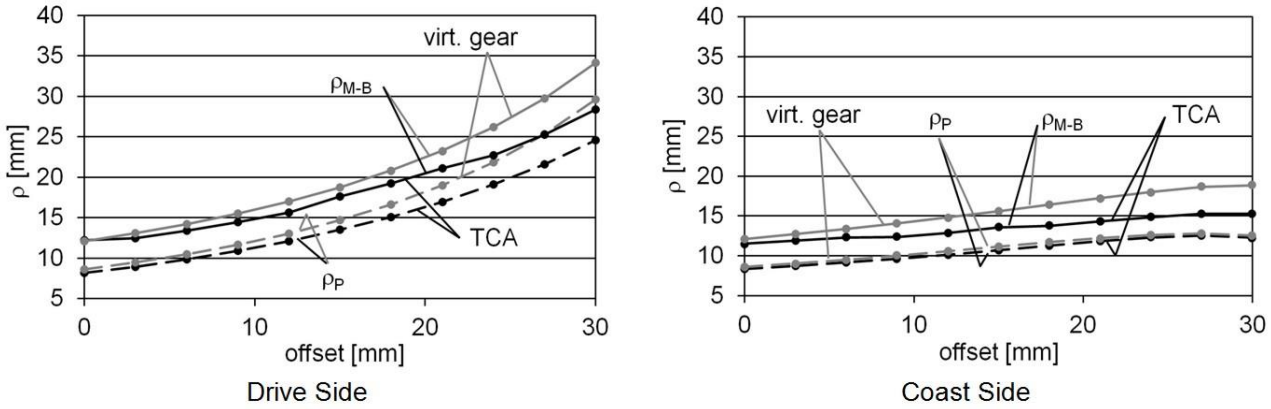

Fig. 14: Relative curvature radius

3.2 Pitting

The new calculation method is based on the calculation of a virtual cylindrical gear that is generated from the bevel or hypoid gear set. The strength values are derived from ISO 6336 [12] for the calculation of helical gears, which has the advantage that the strength values on helical gears are statistically well ensured.

Nominal contact stress, σ_{H0}

$$\sigma_{H0} = \sqrt{\frac{F_n}{l_{bm}\rho_{rel}}} Z_{M\text{-}B} Z_{LS} Z_E Z_K \quad (17)$$

with:

$$F_n = \frac{F_{mt1}}{\cos\alpha_n \cos\beta_{m1}} \quad (18)$$

Contact stress, σ_H

$$\sigma_H = \sigma_{H0} \sqrt{K_A K_v K_{H\beta} K_{H\alpha}} \le \sigma_{HP} \quad (19)$$

Permissible contact stress, σ_{HP}

$$\sigma_{HP} = \sigma_{H\,lim}\, Z_{NT} Z_X Z_L Z_v Z_R Z_W Z_S Z_{Hyp} \quad (20)$$

Fig. 15 shows the calculated results for the endurance limits T_{1lim} of the tests by the new method and DIN 3991 [1], ISO 10300 [3] (for bevel gears with a = 0) and Niemann/Winter [11] (for hypoid gears). Per definition the calculated endurance limit is reached when the safety factor becomes S_H = 1, so all methods should determine safety factors of "1" or somewhat below to be on the safe side. As it can be seen there is a quite good correlation of the values calculated by the new method for all regarded offsets. However ISO 10300 [3] determines a too high load capacity for the pinion what is mainly caused by the assumption that 100% of the face width is used. However, for the test gear at this load stage the effective face with was b_{eff} / b = 75%. For an increasing offset Niemann/Winter III [11] calculates a rising load capacity. As the test results showed, this was not true for the examined gears.

Mainly due to the lengthwise sliding the load capacity remained static or was even slightly decreasing (see Fig. 3). This tendency is represented better by the new method where an influence factor for the amount of lengthwise sliding was introduced that is called the **hypoid factor** Z_{Hyp} (see 3.1.2).

Another important factor which was introduced is the **slip factor** Z_S (see 3.1.1) that accounts for the increase of allowable contact stresses when the critical point of action lies in an area of positive slip. Especially at hypoid gears initial pitting at the pinion started in the middle of the flank in an area of positive slip. Because the strength values of ISO 6336 [12] which are used by the new method are only valid for negative slip, they have to be adapted for positive slip by Z_S.

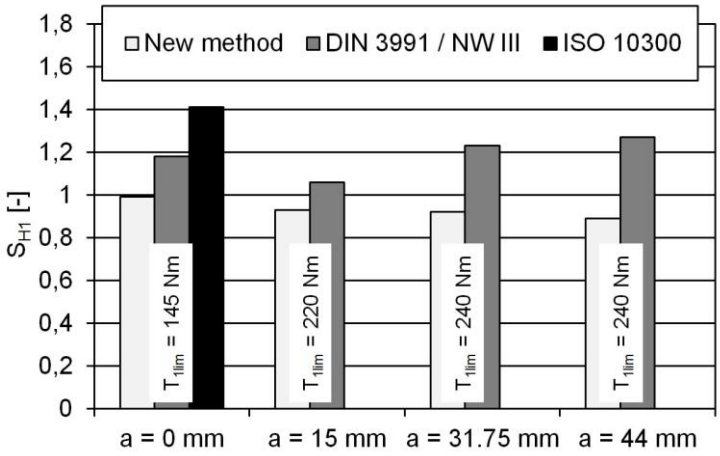

Fig. 15: Calculated safety factors for pitting for the endurance limits of the tests

3.2.1 Slip factor

The bevel slip factor, Z_S, accounts for the increase of surface durability in the flank zone of positive specific sliding versus the zone of negative specific sliding. Experimental investigations on roller tests by Rösch [13] showed decreasing permissible stresses with increasing negative slip. [13] and [14] list possible reasons for that phenomenon. Based on this knowledge the slip factor Z_S was introduced as shown in **Fig. 16** and Eq. (21) and (22).

For bevel gears without offset the change from positive to negative specific sliding is exact on the pitch cone which can be reduced to the mean point for the virtual gear. Whether the critical point of load application for contact stress is above or below the mean point is decided by means of the mid-zone factor, Z_{M-B}. For hypoid gears it is assumed that the mentioned change also takes place at the mean point. So, the bevel slip factor, Z_S, is determined for pinion and wheel depending on the mid-zone factor. In the range of $0{,}98 < Z_{M-B} < 1{,}0$ the bevel slip factor is interpolated (see Fig. 16). If the positive specific sliding applies to the pinion then the negative necessarily applies to the wheel and vice versa.

Slip factor, z_S

$$Z_{S1} = 1{,}175;\ Z_{S2} = 1{,}0 \text{ for } Z_{M\text{-}B} < 0{,}98 \quad (21)$$

$$Z_{S1} = 1{,}0;\ Z_{S2} = 1{,}175 \text{ for } Z_{M\text{-}B} > 1{,}0 \quad (22)$$

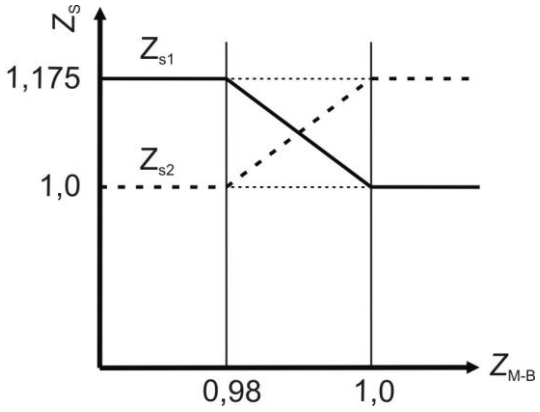

Fig. 16: Slip factor

In the used standard for cylindrical gears ISO 6336 [12] there is no slip influence regarded. The calculated point of load application always lies in the area of negative slip. This is because cylindrical gears with a common design have

- the pitch point close to middle of the flank e.g. due to efficiency reasons. Hence the area of negative sliding is usually considerably big.
- ratios that lead to a maximum of relative curvature radius that lies in the middle area of the patch of contact.
- compared to bevel and hypoid gears small flank form modifications that lead to a equally distributed stress distribution with no or only a small tip or end relief. As a consequence the areas on pinion and wheel close to the tooth root (areas with negative sliding) are highly loaded.

However on bevel and hypoid gears the decisive point of load application may lie in a flank area above the pitch cone with positive specific sliding. Because of the few numbers of teeth the profil shift coefficient has to be chosen considerably high in order to avoid undercut. This may result in a big tooth addendum with positive slip and only a comparably small dedendum with negative slip. The crowning of the gear may lead to a stress distribution where the highest stress lies in the positive slip area. However the permissible stress values in the area of positive slip are bigger than in the area of negative slip, the critical point may lie in the addendum of the pinion tooth. Hence the pitting resistance of the critical point for the pinion has to be evaluated under the influence of positive slip. As a consequence this point lies on the wheel flank in the area with negative specific sliding.

3.2.2 Hypoid factor

The relative motion between the flanks of hypoid gears with nonintersecting axes leads to a sliding component lengthwise the contact line which is directed parallel to the contact line. However helical gears and bevel gears without offset have only a sliding component that is perpendicular to the contact line. Therefore the influence of the lengthwise sliding on the pitting resistance has to be taken into account when the strength values of helical gears should be used for the calculation of hypoid gears. Whereas the amount of lengthwise sliding is approximately constant the perpendicular sliding component is scaled significantly along the tooth profile similar to helical gears. For this reason only the lengthwise component has to be regarded to evaluate the different sliding conditions on hypoid gears in comparison to helical gears. This component leads to higher sliding velocities and causes therefore higher temperatures in the contact point.

As Fig. 3 illustrates, the permissible stresses are decreasing with an increasing offset and a so increasing sliding component parallel to the contact line. Based on the test results the hypoid factor Z_{Hyp} was introduced to evaluate the lengthwise sliding on hypoid gears. Z_{Hyp} was empirically determined and should cover the following phenomena:

1) Influence of the contact temperature on the lubricating film thickness.
2) Influence of the contact temperature on the function of the oil.
3) Influence of the temperature on the material strength.
4) Influence of the temperature distribution on the thermal stresses.
5) Influence on the fracture mechanics on the surface.

The hypoid factor is calculated according to Eq. (23). Hereby the sliding velocity parallel to the contact line v_{gpar} is assumed to have a negative influence on the pitting resistance as described above. The reference value is the sum of the tangential velocities perpendicular to the contact line $v_{\Sigma vert}$ (see **Fig. 18**). These components are considered to have a positive effect on the pitting resistance because of their influence on the oil film thickness. The ratio of both components is an indicator for the different temperature and oil film behaviour of hypoid gears in comparison to cylindrical gears and bevel gears without offset. As **Fig. 17** shows the hypoid factor is $Z_{Hyp} = 1$ for bevel gears with intersecting axes and becomes smaller for higher offsets. For practical applications the lower limit of $Z_{Hyp} = 0.6$ is usually not reached.

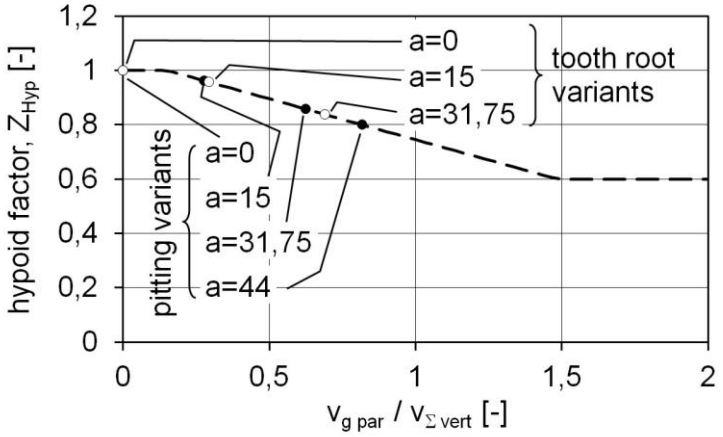

Fig. 17: Hypoid factor

Hypoid factor, σ_{H0}

$$Z_{Hyp} = 1 - 0{,}3\left(\frac{v_{g\,par}}{v_{\Sigma\,vert}} - 0{,}15\right) \quad \text{with } 0{,}6 < Z_{Hyp} < 1{,}0 \qquad (23)$$

Sliding velocity parallel to the contact line, v_{gpar}

$$v_{g\,par} = v_g \cos|\beta_B| \qquad (24)$$

Sliding velocity in P, v_g

$$v_g = v_{mt1}\cos\beta_{m1}(\tan\beta_{m1} - \tan\beta_{m2}) \quad (25)$$

The sum of velocities vertical to the contact line, $v_{\Sigma vert}$

$$v_{\Sigma\,vert} = v_\Sigma \sin(\omega_\Sigma + |\beta_B|) \quad (26)$$

Sum of velocities, v_Σ

$$v_\Sigma = \sqrt{v_{\Sigma h}^2 + v_{\Sigma l}^2} \quad (27)$$

Sum of velocities in profile direction, $v_{\Sigma h}$

$$v_{\Sigma h} = |2\, v_{mt1}\cos\beta_{m1}\sin\alpha_n| \quad (28)$$

Sum of velocities in lengthwise direction

$$v_{\Sigma l} = \left| v_{mt1}\left(\sin\beta_{m1} + \frac{\sin\beta_{m2}\cos\beta_{m1}}{\cos\beta_{m2}}\right)\right| \quad (29)$$

Auxiliary angle, ω_Σ

$$\omega_\Sigma = \left|\arctan\left(\frac{v_{\Sigma h}}{v_{\Sigma l}}\right)\right| \quad (30)$$

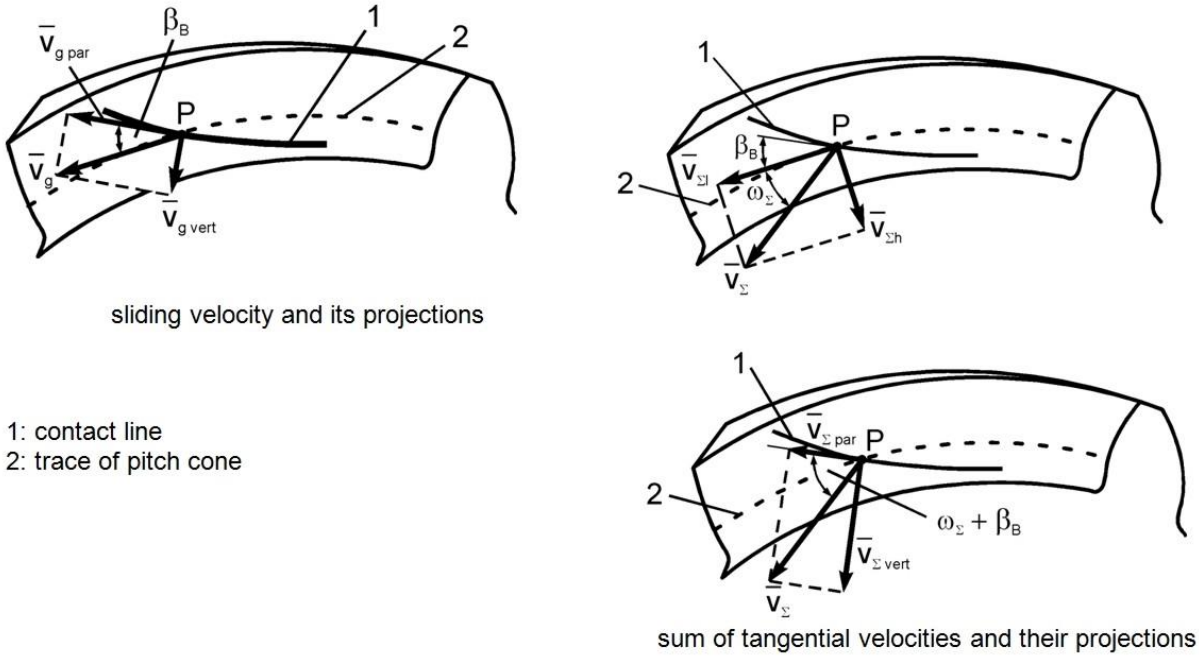

Fig. 18: Velocity conditions show on a pinion flank in mean point P

3.3 Tooth root breakage

As the new method for pitting the calculation of the load capacity for bending is also based on the analysis of the virtual cylindrical gear according to 3.1. The strength values are derived from the standard ISO 6336 [12] for helical gears what is again advantageous for the statistic funding. The influence of different pressure angles as well as the influence of the limit pressure angle is considered. By eq. (31) and (32) the tooth root stress in the decisive mesh position is determined. The permissible stress acc. eq. (33) is equivalent to the current version of ISO 10300 [3].

Nominal tooth root stress, σ_{F0}

$$\sigma_{F0} = \frac{F_{vmt}}{b_v\, m_{mn}} Y_{Fa} Y_{Sa} Y_\varepsilon Y_{BS} Y_{LS} \quad (31)$$

Tooth root stress, σ_F

$$\sigma_F = \sigma_{F0} K_A K_v K_{F\beta} K_{F\alpha} < \sigma_{FP} \quad (32)$$

Permissible tooth root stress, σ_{FP}

$$\sigma_{FP} = \sigma_{FE} Y_{NT} Y_{\delta\,rel\,T} Y_{R\,rel\,T} Y_X \quad (33)$$

Fig. 19 shows the comparison of the calculated results for the endurance limits T_{1lim} of the bending tests. The new method is valid for bevel gears with and without offset, DIN 3991 [1] and ISO 10300 [3] are only applicable on bevel gears with a = 0 and Niemann/Winter III [11] is only accredited for hypoid gears. The calculated endurance limit is reached again when the safety factor becomes $S_F = 1$, so all methods should determine ideally safety factors slightly below "1" to be on the safe side. For the bevel gears without offset all regarded methods are similar in scale. However for hypoid gears Niemann/Winter III [11] shows tendency to have lower load capacity for increasing offsets.

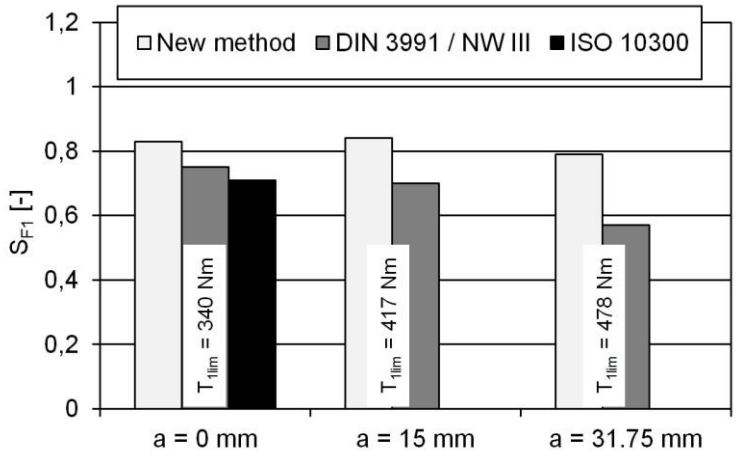

Fig. 19: Calculated safety factors for bending for the endurance limits of the tests

4 Summary

At FZG (Gear Research Centre, Munich, Germany) systematic investigations have been carried out in order to develop a new calculation method for the pitting and bending load capacity of bevel and hypoid gears [15], [16]. By means of a huge number of test gears the new calculation method was statistically ensured as far as possible.

On basis of the current version of ISO 10300 [3] that is only valid for bevel gears with intersecting axes (non hypoid) a new standard capable method was developed for the calculation of bevel and hypoid gears. The proposed virtual cylindrical gear has the same geometry than ISO 10300 [3], AMGA 2003 [2] or DIN 3991 [1] for bevel gears without offset. Because it is essential for the calculation of load capacity that the mesh conditions of hypoid gears are represented sufficiently by the virtual gears the effect of the limit pressure angle was taken into account. It describes the unbalance in mesh on drive and coast side and influences the radii of relative curvature, the inclination of the contact line, the overlap ratio etc.

For the rating of pitting resistance the hypoid factor Z_{Hyp} was introduced to consider the effect of the lengthwise sliding component of hypoid gears on the permissible contact stress in comparison to bevel gears without offset that have only a sliding component perpendicular to the contact line. Because of the necessity to calculate in the area of positive sliding the strength values that are only valid under negative slip have to be adapted. According to test results on discs the slip factor Z_S accounts for the increase of strength in the area of positive slip. As shown before the recalculation of the pitting test is in good agreement regarding the endurance limit of the test gears.

For the rating of bending it is now possible to consider different pressure angles on both flanks, even on bevel gears without offset. In comparison to Niemann/Winter III [11] the increasing load capacity on hypoid pinions for higher offsets is now better represented.

Meanwhile the newly developed calculation method is widely-used in the manufacturing industry. For that reason it is currently introduced in the revision of ISO 10300 [3] as method B1 beside method B2 based on the AGMA calculation method for bevel and hypoid gears.

5 References

[1] DIN 3991: *Tragfähigkeitsberechnung von Kegelrädern ohne Achsversetzung*, Teil 1-4, 1988.

[2] ANSI/AGMA 2003-B97: *Rating the Pitting Resistance and Bending Strength of Generated Straight Bevel, Zerol Bevel and Spiral Bevel Gear Teeth*. American Gear Manufacturers Association, Alexandria, Virginia, 1997.

[3] ISO 10300: *Calculation of Load Capacity of Bevel Gears*. Part 1 2001, Part 2-3 2003.

[4] Paul, M.: *Einfluss von Balligkeit und Lageabweichungen auf die Zahnfußbeanspruchung spiralverzahnter Kegelräder.* Diss. TU München, 1982.

[5] Vollhüter, F.: *Einfluss der Achsversetzung auf die Grübchen- und Zahnfußtragfähigkeit von sprialverzahnten Kegelrädern.* Diss. TU München, 1992.

[6] Fresen, G.: *Einfluss des Achsversatzes auf die Tragfähigkeit von Hypoid- und Kegelgetrieben.* Diss. TU München, 1981.

[7] Hutschenreiter, B.: *Ergänzung der Berechnungsmöglichkeit von BECAL für Flanken mit negativem Höhenballigkeitsradius und Kopfrücknahme.* Abschlussbericht und Handbuchergänzung D zur Version 3.4.0. FVA-Forschungsheft Nr. 548, Forschungsvereinigung Antriebstechnik e.V., 2007.

[8] Shitpelman, B. A.: *Design and Manufacture of Hypoid Gears*. John Wiley & Sons Inc., New York, 1978.

[9] Wildhaber, E.: *Basic Relationship of Hypoid Gears*. American Machinist Vol. 90 No. 4-11., 1946.

[10] ISO 23509: *Bevel and Hypoid Gear Geometry*, 2006.

[11] Niemann, G.; Winter, H.: *Maschinenelemente*. Band 3, Springer-Verlag Berlin Heidelberg New York, 1986.

[12] ISO 6336: *Calculation of Load Capacity of Spur and Helical Gears.* Parts 1-3, 5, 1996.

[13] Rösch, H.: *Untersuchungen zur Wälzfestigkeit von Rollen – Einfluss von Werkstoff, Wärmebehandlung und Schlupf.* Diss. TU München, 1976.

[14] Hertter, T.: *Rechnerischer Festigkeitsnachweis der Ermüdungstragfähigkeit vergüteter und einsatzgehärteter Stirnräder.* Diss. TU München, 2003.

[15] Wirth, Ch.: *Entwicklung eines Berechnungsverfahrens zur Grübchen- und Zahnfußtragfähigkeit von Hypoidrädern.* Forschungsvereinigung Antriebstechnik e.V., Heft 887, Frankfurt 2009.

[16] Wirth, Ch.: *Zur Tragfähigkeit von Kegelrad- und Hypoidgetrieben.* Diss. TU München, 2008.

6 Symbols

Symbol	Description or term
A	load distribution – area of semi-ellipse at middle line of contact
b	face width
b_v	face width of virtual cylindrical gears
b_{eff}	effective face width (e.g. measured length of contact pattern)
$b_{v\,eff}$	effective face width of virtual cylindrical gears
d_m	mean pitch diameter
d_e	outer pitch diameter
d_v	reference diameter of virtual cylindrical gear
d_{va}	tip diameter of virtual cylindrical gear
d_{vf}	root diameter of virtual cylindrical gear
d_{vb}	base diameter of virtual cylindrical gear
e	exponent for the distribution of the load peaks along the lines of contact
f	distance to a contact line
f_{max}	maximum distance to middle contact line
F_n	nominal normal force
F_{nt}	nominal tangential normal force
F_{mt}	nominal tangential force at reference cone at mid face width
F_{vmt}	tangential force of virtual cylindrical gears
$g_{v\alpha}$	length of path of contact of virtual cylindrical gear
h_{am}	mean addendum
h_{fm}	mean dedendum
K_A	application factor
$K_{F\alpha}$	transverse load factor for bending stress
$K_{F\beta}$	face load factor for bending stress
$K_{H\alpha}$	transverse load factor for contact stress
$K_{H\beta}$	face load factor for contact stress
K_V	dynamic factor
l_{b0}	theoretical length of contact line
l_{bm}	theoretical length of middle contact line
m_{mn}	mean normal module
p	peak load
p_{max}	maximum peak load
p*	related peak load
p_{vet}	transverse base pitch of virtual cylindrical gear
P	calculation point (mean)
R_m	mean cone distance
S_F	safety factor for bending stress (against breakage)
S_H	safety factor for contact stress (against pitting)
T_{1lim}	endurance limit of tests for pinion

Symbol	Description or term
v_{mt}	tangential speed at reference cone at mid face width
v_g	sliding velocity
v_{gpar}	sliding velocity parallel to the contact line
v_Σ	sum of velocities
$v_{\Sigma vert}$	sliding velocity vertical to the contact line
$v_{\Sigma h}$	sum of velocities in profile direction
$v_{\Sigma l}$	sum of velocities in lengthwise direction
x_{hm}	profile shift coefficient
Y_{BS}	bevel spiral angle factor
Y_ε	contact ratio factor (tooth root) acc. ISO 10300
$Y_{\delta\ rel\ T}$	relative sensitivity factor acc. ISO 10300
Y_{Fa}	tooth form factor for load application at tip
Y_{LS}	load sharing factor (bending)
Y_{NT}	life factor of the standard test gear acc. ISO 10300
$Y_{R\ rel\ T}$	relative surface factor acc. ISO 10300
Y_{Sa}	stress correction factor for load application at tooth tip acc. ISO 10300
Y_X	size factor for tooth root stress acc. ISO 10300
Z_E	elasticity factor acc. ISO 10300
Z_{Hyp}	hypoid factor
Z_K	bevel gear factor
Z_{LS}	load sharing factor
Z_{M-B}	mid zone factor acc. ISO 10300
Z_{NT}	life factor of the standard test gear acc. ISO 10300
Z_R	roughness factor for contact stress acc. ISO 10300
Z_S	bevel slip factor
Z_v	speed factor acc. ISO 10300
Z_W	work hardening factor acc. ISO 10300
Z_X	size factor acc. ISO 10300
α_e	effective pressure angle
α_{vet}	transverse pressure angle of virtual cylindrical gear
α_{lim}	limit pressure angle
α_{limt}	transverse limit pressure angle
α_n	generated pressure angle
α_t	pressure angle in transverse section
β_m	mean spiral angle
β_v	helix angle of virtual cylindrical gear
β_{vb}	helix angle at base circle of virtual cylindrical gear
β_B	inclination angle of contact line
δ	pitch angle of bevel gear
γ	auxiliary angle for length of contact line
γ'	projected auxiliary angle for length of contact line

Symbol	Description or term
ϑ_{mp}	auxiliary angle for face width
ρ_{M-B}	radius of relative curvature at decisive point of load application for pitting
ρ_p	radius of relative curvature at calculation point
ρ_{rel}	radius of relative curvature vertical to contact line at virtual cylindrical gears
ρ_t	radius of relative curvature in normal section at bevel gears
σ_{H0}	nominal value of contact stress
σ_H	contact stress
σ_{HP}	permissible contact stress
σ_{Hlim}	allowable stress number for contact stress acc. ISO 10300
σ_F	tooth root stress
σ_{F0}	local tooth root stress
σ_{FP}	permissible tooth root stress
σ_{FE}	allowable stress number (bending) acc. ISO 10300
ω_Σ	angle between sum of velocities and flank lengthwise direction
ζ_m	pinion offset angle in face plane
ζ_{mp}	pinion offset angle in pitch plane
Subscripts	
C	drive side
D	coast side